



Bifurcation Asymmetry of Small Coronary Arteries in Juvenile and Adult Mice

Yundi Feng¹, Xuan Wang¹, Tingting Fan¹, Li Li¹, Xiaotong Sun¹, Wenxi Zhang¹, Minglu Cao¹, Jian Liu^{2*}, Jianping Li^{3*} and Yunlong Huo^{1*}

¹ Department of Mechanics and Engineering Science, College of Engineering, Peking University, Beijing, China, ² Department of Cardiology, Peking University People's Hospital, Beijing, China, ³ Department of Cardiology, Peking University First Hospital, Beijing, China

OPEN ACCESS

Edited by:

Julius Guccione,
University of California, San Francisco,
United States

Reviewed by:

Trevor R. Cardinal,
California Polytechnic State University,
United States
Joakim Sundnes,
Simula Research Laboratory, Norway

*Correspondence:

Jian Liu
drjianliu@163.com
Jianping Li
lijianping@medmail.com.cn
Yunlong Huo
yhuo@pku.edu.cn

Specialty section:

This article was submitted to
Computational Physiology and
Medicine,
a section of the journal
Frontiers in Physiology

Received: 01 January 2018

Accepted: 23 April 2018

Published: 15 May 2018

Citation:

Feng Y, Wang X, Fan T, Li L, Sun X,
Zhang W, Cao M, Liu J, Li J and
Huo Y (2018) Bifurcation Asymmetry
of Small Coronary Arteries in Juvenile
and Adult Mice. *Front. Physiol.* 9:519.
doi: 10.3389/fphys.2018.00519

Background: Microvascular bifurcation asymmetry is of significance for regulation of coronary flow heterogeneity during juvenile and adult growth. The aim of the study is to investigate the morphometric and hemodynamic variation of coronary arterial bifurcations in mice of different ages.

Methods: Pulsatile blood flows were computed from a Womersley-type model in the reconstructed left coronary arterial (LCA) trees from Micro-CT images in normal mice at ages of 3 weeks, 6 weeks, 12 weeks, 5–6 months, and >8 months. Diameter and flow ratios and bifurcation angles were determined in each bifurcation of the LCA trees.

Results: The blood volume and inlet flow rate of LCA trees increase and decrease during juvenile and adult growth, respectively. As vessel diameters decrease, the increased ratios of small to large daughter vessel diameters (D_s/D_l) result in more uniform flows and lower velocities. There are significant structure-functional changes of LCA trees in mice of >8 months compared with mice of <8 months. As D_s/D_l increases, the variation trend of bifurcation angle during juvenile growth is different from that during adult growth.

Conclusions: Although inlet flows are different in adult vs. juvenile mice, the adult still have uniform flow and low velocity. This is accomplished through a decrease in diameter. The design ensures ordered dispersion of red cells through asymmetric branching patterns into the capillaries.

Keywords: coronary arterial tree, bifurcation asymmetry, bifurcation angle, advancing age, mouse model

INTRODUCTION

The structure and function of coronary arterial trees undergo changes during normal growth and aging (Wei, 1992; LeBlanc and Hoying, 2016). For example, an increase of vessel density was found in the adult primarily owing to angiogenesis in which new daughter vessel segments grow (sprouting) or split (intussusception) from existing mother segments (Carmeliet and Jain, 2011; LeBlanc and Hoying, 2016). We have recently shown an age-independent exponent in the length-volume scaling law of an entire coronary arterial tree in juvenile and adult mice (Chen et al., 2015) because of fractal-like tree features (Huo and Kassab, 2016). In comparison with the unchanged “global” hierarchy of a vascular tree structure, the “local” branching patterns characterize the age-dependent anatomy of coronary arterial trees and affect flow patterns at junctions

(Huo et al., 2009a; Huo Y. L. et al., 2012). The change of flow patterns can lead to low wall shear stress, high oscillatory shear index, high spacial gradient of wall shear stress, and so on (Huo et al., 2007a, 2008, 2009b). These hemodynamic parameters are related to stagnation, reversal and vortical flows (Asakura and Karino, 1990; Kleinstreuer et al., 2001; Huo et al., 2007a), which result in abnormal biological responses such as dysfunction of endothelial cells, monocyte deposition, elevated wall permeability to macromolecules, particle migration into the vessel wall, smooth muscle cell proliferation, microemboli formation, and so on (Malek et al., 1999; Chiu and Chien, 2011). The current studies of advancing age in the coronary vasculature are generally confined to large epicardial arteries (LeBlanc and Hoying, 2016). To our knowledge, there is, however, lack of studies to show the effects of normal growth and development on the “local” branching patterns in coronary resistance vasculature (vessel diameter <200 μm).

Coronary blood flows in arterioles and small arteries play a fundamental role for regulation of total vascular resistance under physiological and pathological conditions (Chilian et al., 1989; Chilian, 1991; Pries and Secomb, 2005; Reglin et al., 2017). The flows are affected by multiple factors, e.g., Fahraeus-Lindqvist effects, bifurcation laws, and so on (Pries et al., 1995; Gompfer and Fedosov, 2016; Secomb, 2017). Based on the constructal law, Bejan and Lorente indicated that an efficient transport system requires more symmetric bifurcations to keep fractional flows as uniform as possible (Bejan and Lorente, 2010). According to the morphometric measurements, normal arteriolar bifurcations are more symmetric than ischemia-regenerated or tumor-induced branching patterns to ensure ordered dispersion of red cells through the capillary network (Baish and Jain, 2000; Arpino et al., 2017).

The objective of the study is to investigate the changes of bifurcation asymmetry in coronary arterial trees of mice during juvenile and adult growth. We hypothesize that the bifurcation changes of small coronary arteries (i.e., diameter ratio and bifurcation angle) result in more uniform flows and lower velocities as vessel diameters decrease in mice of different ages. The inlet flow rate and blood volume of coronary arterial trees are also assumed to have different variation trends between juvenile and adult growth. To test the hypothesis, we analyzed diameter ratios and bifurcation angles in each bifurcation of coronary arterial trees reconstructed from Micro-CT (μCT) images of mice at ages of 3, 6, 12 weeks, 5-6 months and >8 months. Pulsatile blood flows in each tree were computed from a Womersley-type model (Huo and Kassab, 2006), based on which the flow and velocity ratios were determined in each bifurcation. The significance and limitation of the morphometric and hemodynamic analysis were discussed relevant to the microcirculation.

MATERIALS AND METHODS

Morphometric Data

We have reconstructed coronary arterial trees of ICR (Institute of Cancer Research) mice from μCT images. All animal

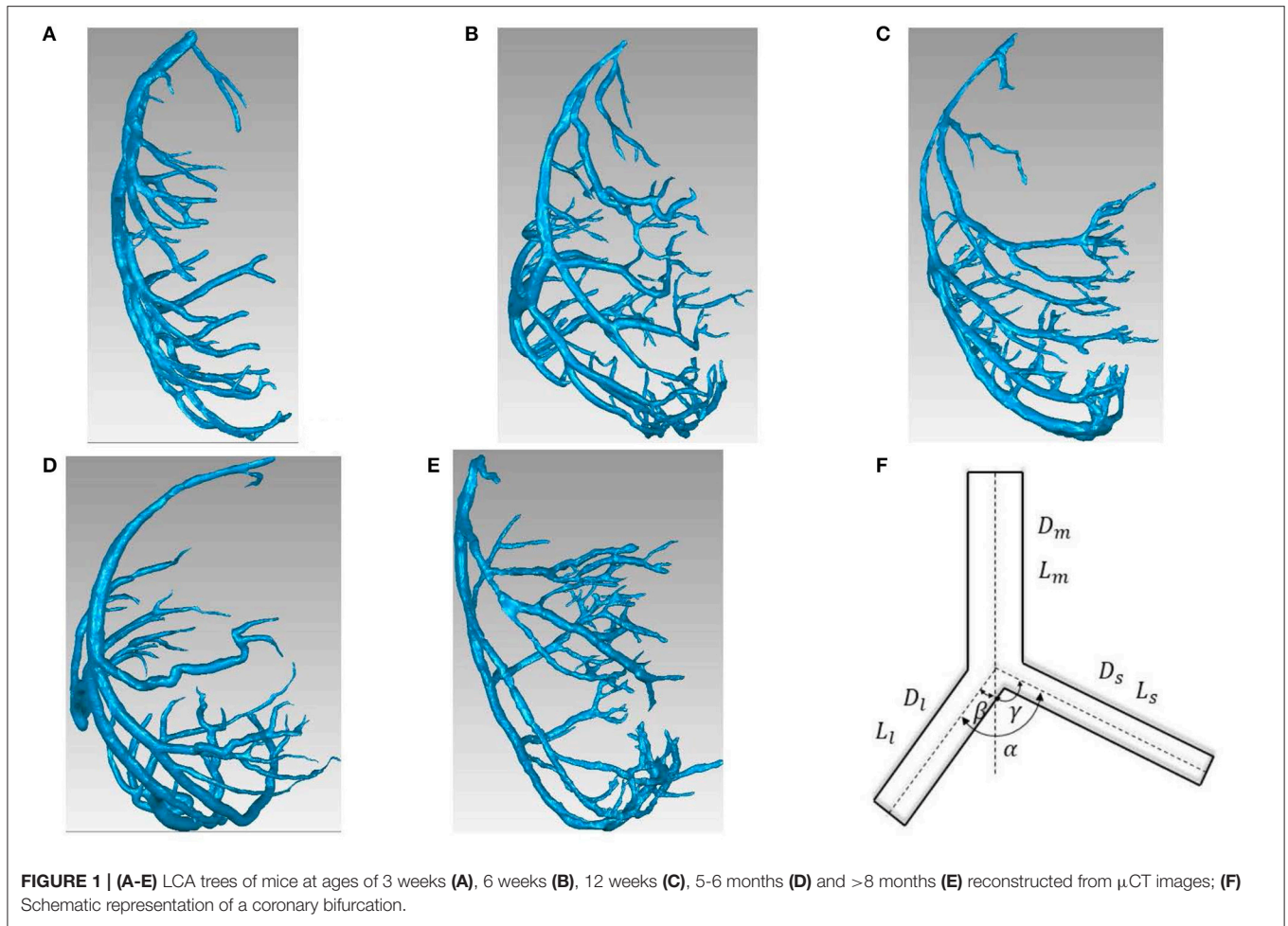
experiments were performed in accordance with Chinese National and Hebei University ethical guidelines regarding the use of animals in research, consistent with the NIH guidelines (Guide for the care and use of laboratory animals) on the protection of animals used for scientific purposes. The experimental protocols were approved by the Animal Care and Use Committee of Hebei University, China.

The reconstructed left coronary arterial (LCA) trees (including 9 LCA trees in 3 weeks group, 9 LCA trees in 6 weeks group, 7 LCA trees in 12 weeks group, 8 LCA trees in 5-6 months group and 9 LCA trees in > 8 months group) were used to analyze the changes in bifurcations of normal mice at different ages (from 3 weeks to >8 months), as shown in **Figures 1A-E**. Similar to a previous study (Chen et al., 2015), animals were anesthetized with pentobarbital sodium (60 mg/Kg) and heparinized with undiluted heparin (1 ml, 1,000 USPU/ml). After midline incision for laparotomy, animals were terminated by injecting an overdose of pentobarbital sodium through the inferior vena cava. The thoracic aorta was perfused with MICROFIL (Flow Tech, Carver, MA) at a constant pressure of 100 mmHg after the termination. The flow of cast solution was zero during the 90 min prior to hardening of cast at a constant pressure of 100 mmHg. The animal was stored in 10% formalin in the refrigerator for 24 h. The hearts were dissected and stored in 10% formalin in refrigerator until μCT scans. Morphometric data of LCA trees (including the diameter and rectangular coordinates of center points which were located in the center on the cross-sectional views of the contour of the 3D vessel) were extracted from μCT images using a gray-scale threshold method (with a low CT-threshold of 100) in the MIMICS software (Materialize, NV, Belgium).

A centerline was formed by a series of center points. Subsequently, the best fit diameter, D_{fit} , was calculated as twice the average radius between the center point and the contour forming the 3D vessel. The blurring of small vessel edges was corrected to yield $D_{correct}$ by fitting a Gaussian distribution function to the line profiles followed by computation of the input square wave. Since a vessel (a segment between two nodes of bifurcation) included 10-80 center points, the length and volume of a vessel were defined as:

$$L = \sum_{i=0}^{N-1} \sqrt{(x_{i+1} - x_i)^2 + (y_{i+1} - y_i)^2 + (z_{i+1} - z_i)^2} \text{ and } V = \sum_{i=0}^{N-1} \left(\frac{\pi D_{correct}^2}{4} \cdot \sqrt{(x_{i+1} - x_i)^2 + (y_{i+1} - y_i)^2 + (z_{i+1} - z_i)^2} \right),$$

where (x, y, z) refers to rectangular coordinates of center points from inlet ($i = 0$) to outlet ($i = N$) of the vessel. The cross-section area (CSA) of a vessel equaled to the intravascular volume divided by the length. A linear least-squares fit of all center points was used to determine the spatial direction of a vessel. The mother, large daughter, and small daughter diameters and lengths, (D_m, L_m) , (D_l, L_l) , and (D_s, L_s) , as well as bifurcation angles were determined at all bifurcations of coronary arterial trees, as shown in **Figure 1F**. The LCA trees with vessel diameter $\geq 40 \mu\text{m}$ (twice the voxel size) were used to reduce the sampling error of the finite discrete grid. Unless otherwise stated, the terminal vessels of μCT -determined LCA trees have diameter $\geq 40 \mu\text{m}$.



Womersley-Type Model

Similar to a previous study (Huo and Kassab, 2006), a mathematical model is used to analyze pulsatile blood flow of coronary arteries in diastole in the absence of vessel tone. The governing equations for flow and pressure in a vessel ($x = 0$ and $x = L$ refer to the inlet and outlet, respectively) can be written as:

$$Q(x, \omega) = a \cdot \cos\left(\frac{\omega x}{c}\right) + b \cdot \sin\left(\frac{\omega x}{c}\right) \quad (1)$$

$$P(x, \omega) = iZ_1 \left[-a \cdot \sin\left(\frac{\omega x}{c}\right) + b \cdot \cos\left(\frac{\omega x}{c}\right) \right] \quad (2)$$

where a and b are arbitrary constants of integration, ω the angular frequency, $c = \sqrt{1 - F_{10}(\alpha)} \cdot c_0$ ($c_0 = \sqrt{\frac{Eh}{\rho R}}$ and α is the Womersley number) the wave velocity, $Y_0 = \frac{A(n)}{\rho c_0}$ the characteristic admittance, $Z_0 = \frac{1}{Y_0}$ the characteristic impedance, and $Z_1 = Z_0 / \sqrt{1 - F_{10}(\alpha)}$. Moreover, we define the impedance and admittance as:

$$Z(x, \omega) = \frac{P(x, \omega)}{Q(x, \omega)} \text{ and } Y(x, \omega) = \frac{Q(x, \omega)}{P(x, \omega)} \quad (3)$$

In a given vessel segment, at $x = 0$ and $x = L$, we have the respective inlet and outlet impedances:

$$Z(0, \omega) = \frac{iZ_1 \cdot b}{a} \text{ and } Z(L, \omega) = \frac{iZ_1 [-a \cdot \sin\left(\frac{\omega L}{c}\right) + b \cdot \cos\left(\frac{\omega L}{c}\right)]}{a \cdot \cos\left(\frac{\omega L}{c}\right) + b \cdot \sin\left(\frac{\omega L}{c}\right)} \quad (4)$$

From Equation (4), we obtain:

$$Z(0, \omega) = \frac{iZ_1 \cdot \sin\left(\frac{\omega L}{c}\right) + Z(L, \omega) \cdot \cos\left(\frac{\omega L}{c}\right)}{\cos\left(\frac{\omega L}{c}\right) + iY_1 \cdot Z(L, \omega) \cdot \sin\left(\frac{\omega L}{c}\right)} \quad (5)$$

Equation (5) was used to calculate the impedance/admittance in a tree from inlet to the terminal vessels.

Method of Solution

The characteristic impedance, characteristic admittance and velocity (including the viscous effect) were first calculated for every vessel segment. We assume that mass is conserved and pressure is continuous at each bifurcation, which may be written as:

$$Q_m(\omega) = Q_l(\omega) + Q_s(\omega) \text{ and } P_m(\omega) = P_l(\omega) = P_s(\omega) \quad (6)$$

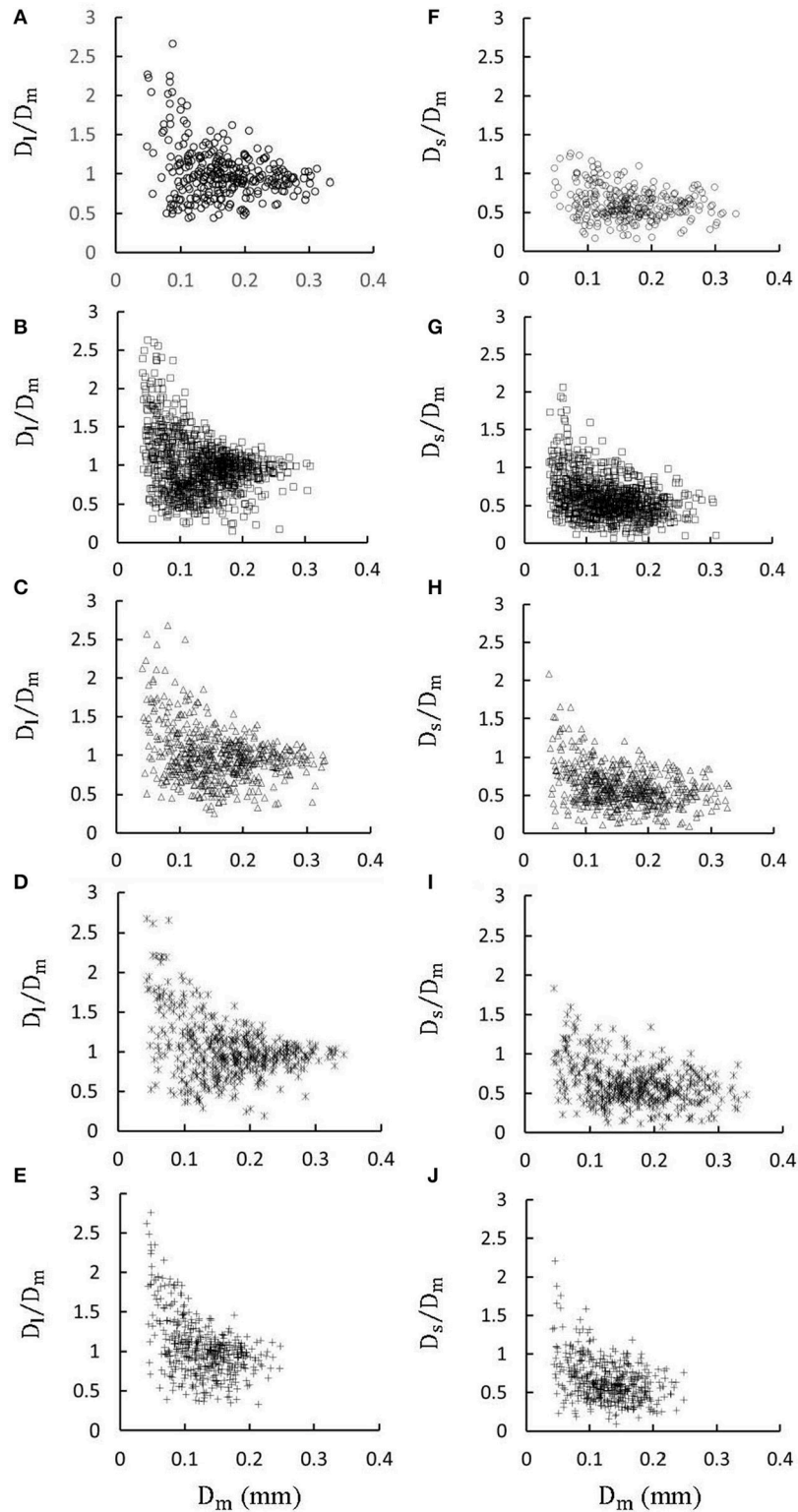
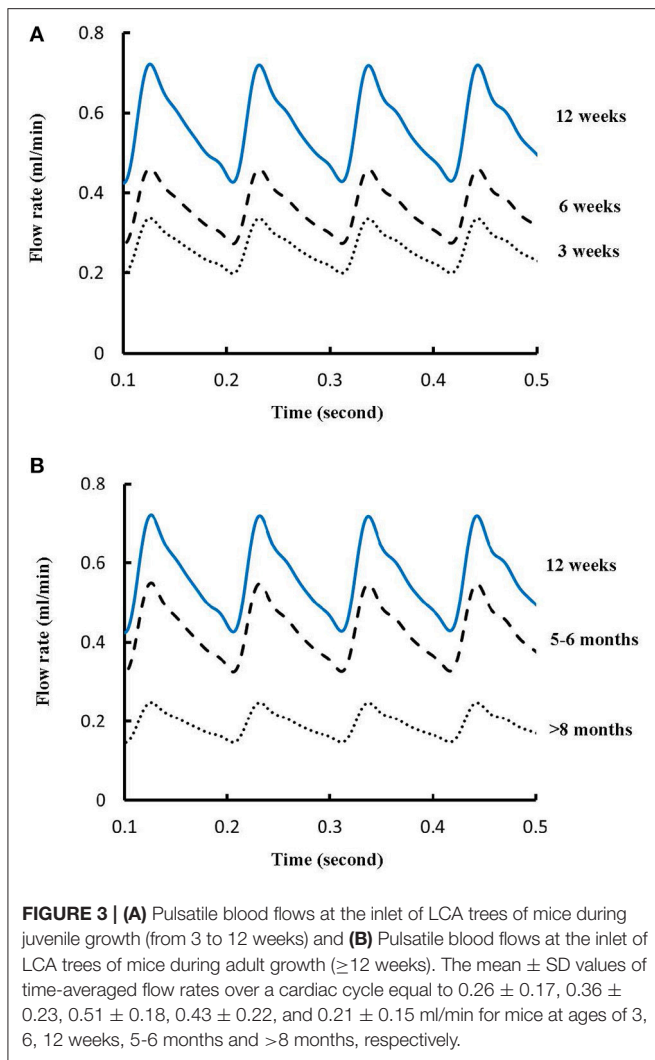


FIGURE 2 | (A–E) Relationship between D_l/D_m (diameter ratio of large daughter to mother vessels) and D_m (diameter of mother vessel) in all bifurcations of mice at ages of 3 weeks (A), 6 weeks (B), 12 weeks (C), 5–6 months (D) and >8 months (E); (F–J) Relationship between D_s/D_m (diameter ratio of small daughter to mother vessels) and D_m in all bifurcations of mice at ages of 3 weeks (F), 6 weeks (G), 12 weeks (H), 5–6 months (I), and >8 months (J). There is significant difference of D_l/D_m and D_s/D_m between mice of >8 months and 3 weeks, between mice of >8 months and 6 weeks, between mice of >8 months and 12 weeks, and between mice of >8 months and 5–6 months while there is no statistical difference between mice of other ages.

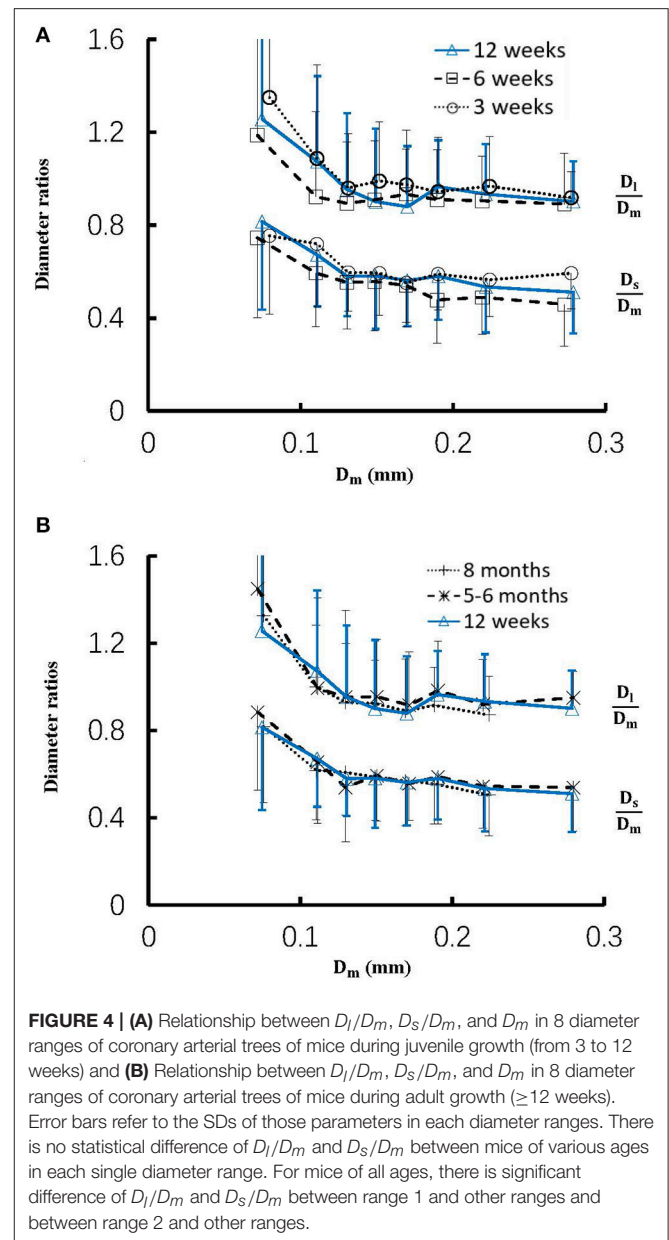


From Equation (6), we obtain:

$$Y_m(L, \omega) = Y_l(0, \omega) + Y_s(0, \omega) \quad (7)$$

Once the terminal impedance/admittance is computed, we proceed backwards to iteratively calculate the impedance/admittance in the entire coronary tree by using Equations (5) and (7) similar to a previous study (Huo and Kassab, 2006). The aortic pressure was obtained from a previous study (Huo et al., 2008) and discretized by a Fourier transformation to determine the constants a and b in Equations (1) and (2). The flow and pressure were then calculated by using Equations (1) and (2).

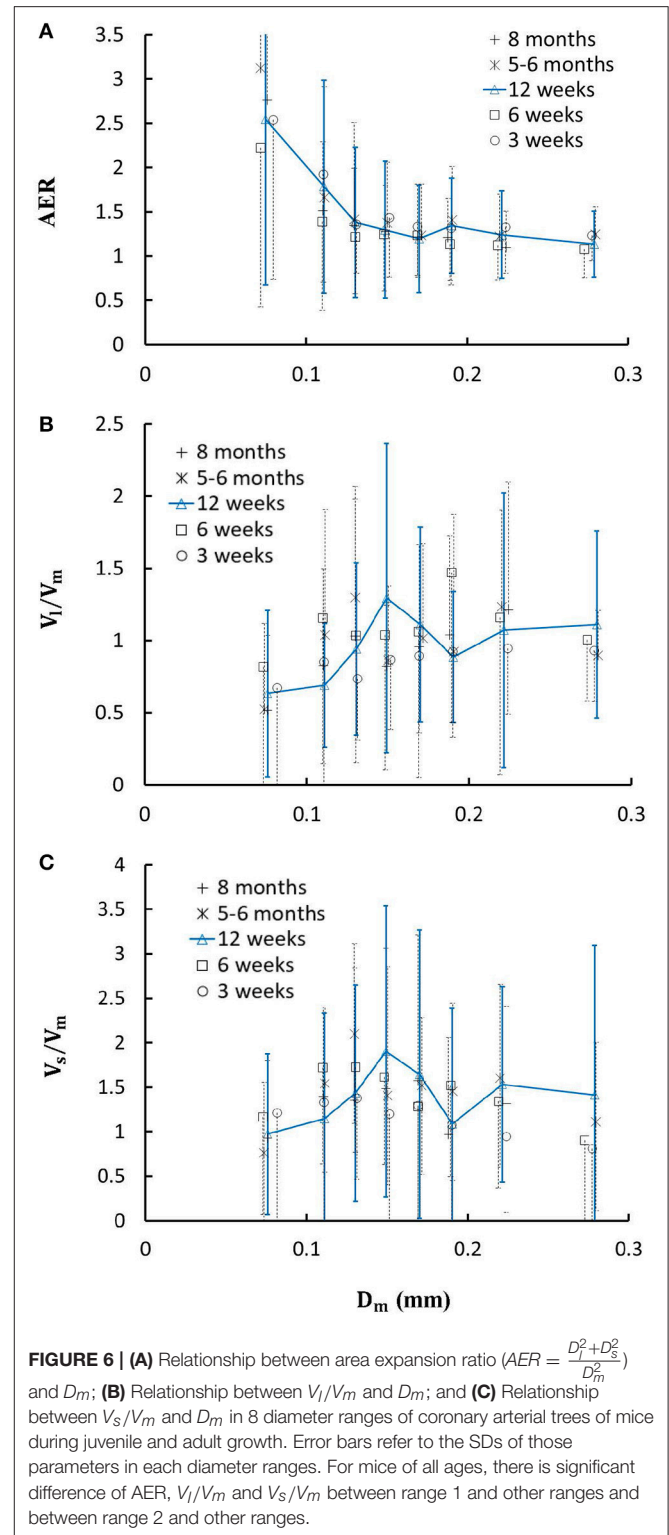
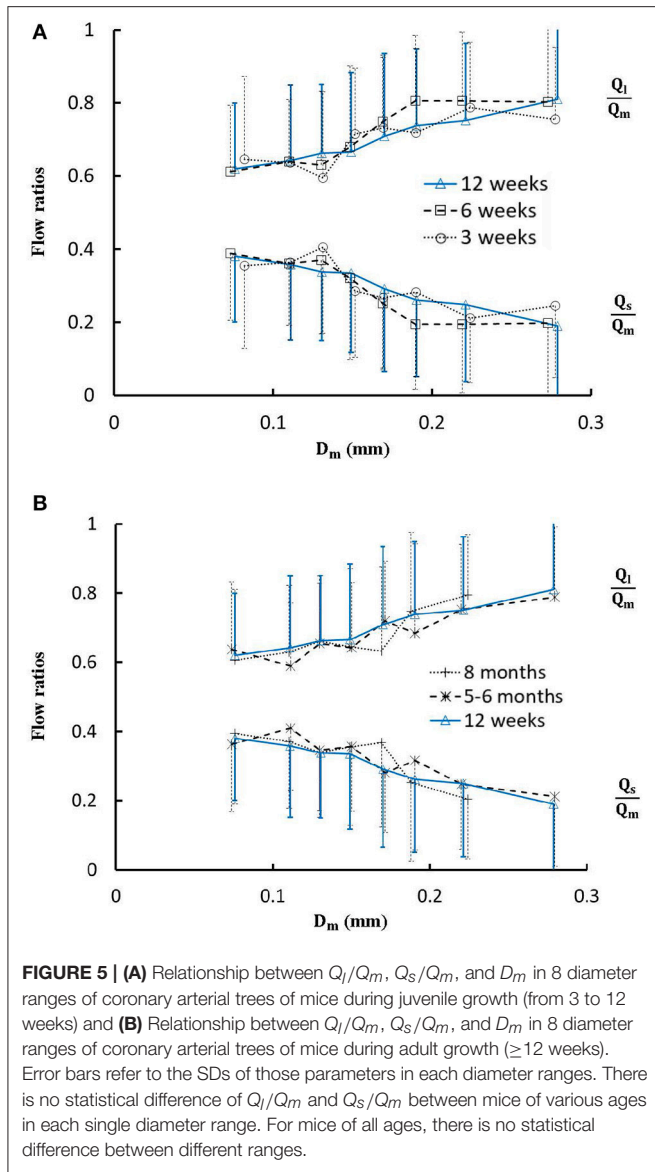
The blood flow density (ρ) in coronary arteries was assumed to be 1.06 g/cm^3 (Chen et al., 2016; Fan et al., 2016; Yin et al., 2016). The variation of viscosity (μ) with vessel diameter and hematocrit was based on Pries' viscosity model (Pries et al., 1992). The coronary wall thickness was assumed to be one-tenth of the vessel diameter. The static Young's modulus was $\sim 8.0 \times 10^6$ (dynes/cm²) and the dynamic Young's modulus was also



considered consistent with the previous study (Huo and Kassab, 2006). Symmetric arteriolar subtrees were pasted to all terminal vessels. A symmetric arteriolar subtree was constructed from the terminal vessel down to the first capillaries, based on two scaling relationships, $DR = 2^{\frac{-1}{1.07+2}}$ and $LR = 2^{\frac{-1}{3-0.42}}$ (DR and LR refer to the diameter and length ratio) (see Table 2 in Huo and Kassab, 2012a). The outlet impedances at the first capillaries were computed by the steady value; i.e., $\frac{128\mu_{capillary}L_{capillary}}{\pi D_{capillary}^4}$ ($\text{g} \cdot \text{sec/cm}^4$).

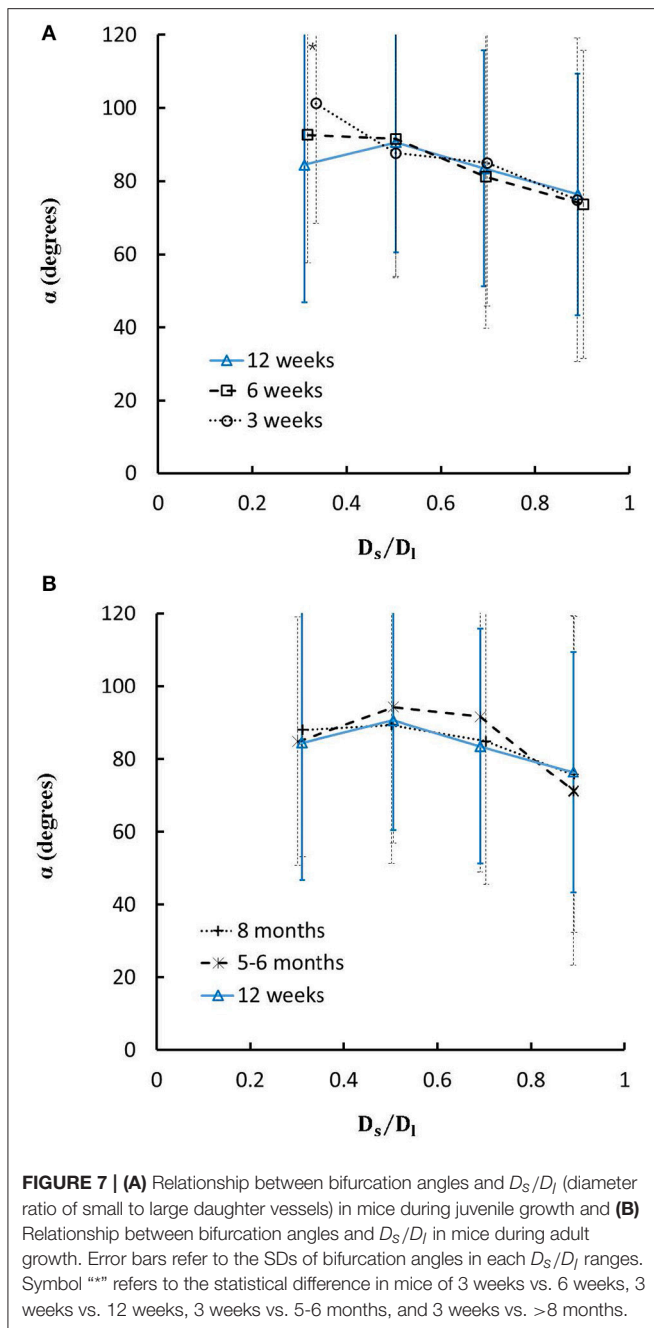
Statistical Analysis

The fraction of volumetric blood flow is mainly determined by diameter ratios ($\frac{D_l}{D_m}$, $\frac{D_s}{D_m}$, and $\frac{D_s}{D_l}$) while the change of flow velocities from mother to daughter vessels is characterized by



the area expansion ratio ($AER = \frac{D_l^2 + D_s^2}{D_m^2}$) (VanBavel and Spaan, 1992; Kaimovitz et al., 2008). Bifurcation angle in small arteries regulates the spacial heterogeneity of coronary blood flow albeit it is a critical risk factor for atherosclerotic plaques and stenting restenosis in large epicardial coronary arteries (Huo et al., 2012b; Huo Y. et al., 2012a). Hence, similar to previous studies (Huo et al., 2007b; Huo and Kassab, 2012b), diameter ratios ($\frac{D_l}{D_m}$, $\frac{D_s}{D_m}$, and $\frac{D_s}{D_l}$), area expansion ratios ($AER = \frac{D_l^2 + D_s^2}{D_m^2}$), flow ratios ($\frac{Q_l}{Q_m}$, $\frac{Q_s}{Q_m}$, and $\frac{Q_s}{Q_l}$), and velocity ratios ($\frac{V_l}{V_m}$, $\frac{V_s}{V_m}$, and $\frac{V_s}{V_l}$) in a LCA tree were analyzed in eight mother diameter (i.e., D_m) ranges as: Range 1 ($<100 \mu\text{m}$), Range 2 ($100\text{-}120 \mu\text{m}$), Range 3 ($120\text{-}140 \mu\text{m}$), Range 4 ($140\text{-}160 \mu\text{m}$), Range 5 ($160\text{-}180 \mu\text{m}$), Range 6 ($180\text{-}200 \mu\text{m}$), Range 7 ($200\text{-}250 \mu\text{m}$) and Range 8 ($\geq 250 \mu\text{m}$). Moreover, bifurcation angles in a LCA

tree were summarized in four $\frac{D_s}{D_l}$ ranges as: Range 1 (<0.4), Range 2 ($0.4\text{-}0.6$), Range 3 ($0.6\text{-}0.8$) and Range 4 (≥ 0.8). The mean and standard deviation (mean \pm SD) were computed by averaging over all bifurcations in each group. Two Way Repeated



Measures ANOVA (SigmaStat 3.5) was used to compare those morphometric and hemodynamic parameters in bifurcations between different ages and between different diameter ranges, where $p < 0.05$ represented a statistically significant difference.

RESULTS

Figures 1A-E show LCA trees of mice at ages of 3, 6, 12 weeks, 5-6 months, and >8 months reconstructed from μ CT images. Accordingly, the LCA trees have blood volumes of 7.1 ± 4.1 , 9.9 ± 3.7 , 16.1 ± 4.7 , 13.8 ± 4.0 , and 5.5 ± 3.4 ($\times 10^{-4}$) cm^3

(averaged over all LCA trees in each group) and the animals have body weights (BW) of 11.0 ± 0.8 , 17.4 ± 1.5 , 37.6 ± 3.9 , 36.1 ± 4.1 , and 38.1 ± 4.8 g (averaged over all animals in each group). **Figures 2A-E** show the changes of D_l/D_m (diameter ratio of large daughter to mother vessels) as a function of D_m (diameter of mother vessel) in all bifurcations of mice at different age groups. **Figures 2F-J** show the corresponding changes of D_s/D_m (diameter ratio of small daughter to mother vessels) with D_m . A comparison in all bifurcations shows that mice of >8 months have significant difference of D_l/D_m and D_s/D_m from mice of <8 months ($p < 0.05$ between mice of >8 months and 3 weeks, between mice of >8 months and 6 weeks, between mice of >8 months and 12 weeks, and between mice of >8 months and 5-6 months) despite no statistical difference between mice of other ages. **Figures 3A,B** show pulsatile blood flows (waves averaged over all mice at the same age) at the inlet of LCA trees of mice during juvenile and adult growth, respectively. The time-averaged flow rate over a cardiac cycle has mean \pm SD values of 0.26 ± 0.17 , 0.36 ± 0.23 , 0.51 ± 0.18 , 0.43 ± 0.22 , and 0.21 ± 0.15 ml/min for mice at ages of 3, 6, 12 weeks, 5-6 months and >8 months, which are proportional to the blood volumes of LCA trees. Similar to the changes of D_l/D_m and D_s/D_m , a comparison in all bifurcations shows mice of >8 months have significant difference of Q_l/Q_m and Q_s/Q_m from mice of <8 months despite no statistical difference between mice of other ages. Moreover, there is significant difference of V_l/V_m and V_s/V_m between mice of 3 and 6 weeks, between mice of 3 and 12 weeks, and between mice of 3 weeks and 5-6 months as well as between mice of >8 months and 6 weeks, between mice of >8 months and 12 weeks, and between mice of >8 months and 5-6 months.

Figure 4 shows the changes of diameter ratios as a function of mother diameter during juvenile and adult growth while **Figure 5** shows the changes of flow ratios. **Figures 6A-C** show the relationships between AER and D_m , between V_l/V_m and D_m , and between V_s/V_m and D_m in coronary arterial trees of mice during juvenile and adult growth. A comparison of those parameters in each single diameter range shows no statistical difference between mice of different ages. As mother vessel diameter increases in mice of 3, 6, 12 weeks, 5-6 months and >8 months, AER and diameter ratios (D_l/D_m and D_s/D_m) decrease abruptly when $D_m < 140$ μm and remain relatively unchanged when $D_m \geq 140$ μm ($p < 0.05$ between range 1 and other ranges and between range 2 and other ranges). Moreover, D_s/D_l values when $D_m < 140$ μm are slightly higher than those when $D_m > 200$ μm . There are gradual increase and decrease of Q_l/Q_m and Q_s/Q_m , respectively, with the increase of mother vessel diameter. There is an abrupt decrease of V_l/V_m , and V_s/V_m as mother vessel diameter decreases from 140 to 40 μm ($p < 0.05$ between range 1 and other ranges and between range 2 and other ranges).

On the other hand, **Figures 7A,B** show the relationships between the measured bifurcation angles ($\alpha_{measured}$) and D_s/D_l during juvenile and adult growth, respectively. There is a monotonical decrease of $\alpha_{measured}$ with the increase of D_s/D_l at ages of 3 and 6 weeks, but a parabolic curve with peak values ($\sim 90^\circ$) when $D_s/D_l = 0.5$ at ages of 12 weeks, 5-6 months, and >8 months ($p < 0.05$ for 3 weeks vs. 6 weeks, 3 weeks vs. 12

weeks, 3 weeks vs. 5-6 months, and 3 weeks vs. >8 months when $D_s/D_l < 0.4$).

DISCUSSION

The present study used a Womersley-type mathematical model to compute pulsatile blood flows in LCA trees of mice. The computed flow rates at the inlet of LCA trees vary in the range of 0.2-0.5 ml/min in agreement with the Doppler measurements (Teng et al., 2016). The inlet flow rate and blood volume of LCA trees increase in mice from 3 to 12 weeks and decrease during adult growth. Myocardial flows were estimated to be 9.45, 8.28, 5.43, 4.76, and 2.21 ml/min/g, respectively, in mice of 3, 6, 12 weeks, 5-6 months and >8 months. Myocardial flows in mice of <8 months are significantly higher than those in porcine (~2.25 mL/min/g in Huo et al., 2009a). On the other hand, the waveform is preserved at the inlet of LCA trees in diastole in the absence of vessel tone during juvenile and adult growth, as shown in **Figure 3**. Furthermore, **Figure 5** showed the development of relatively uniform flows as vessel diameters decrease from the inlet to 40 μm in LCA trees of mice, which agrees with previous findings (Bejan and Lorente, 2010). This is mainly attributed to the design of branching patterns as shown in **Figures 1, 4**.

A key finding of the study is that diameter ratios (D_l/D_m and D_s/D_m) and AER when $40 \mu\text{m} \leq D_m < 140 \mu\text{m}$ in mice are significantly higher than those in porcine (Kaimovitz et al., 2008) despite their similarity at $140 \mu\text{m} \leq D_m < 350 \mu\text{m}$, which leads to an abrupt decrease of velocity ratios (V_l/V_m and V_s/V_m) as vessel diameters decrease from 140 to 40 μm in **Figure 6** (Kassab, 2005). Mice at the age of <8 months have significantly higher myocardial flows (>two-fold) than large animals. Owing to the proportional relation between myocardial flow and metabolic rate, a significant increase of diameter ratios and AER reduces the flow velocity in vessels of $40 \mu\text{m} \leq D_m < 140 \mu\text{m}$ to satisfy the metabolism in the mouse heart compared with large animals in that microvascular blood flow per unit of time is to ensure the needed exchange of substances between tissue and blood compartments (Jacob et al., 2016). We also demonstrated a comparison of diameter and flow ratios to show the effects of normal growth and development on morphometry and hemodynamics of LCA trees of mice. The statistical analysis at all bifurcations showed significant difference of diameter and flow ratios between mice of >8 months and others as well as no statistical difference between mice of <8 months. Myocardial flows in mice of >8 months were also significantly lower than others. Diameter ranges 1-7 showed no statistical difference between mice of different ages while mice of >8 months have no arteries in diameter range 8 ($\geq 250 \mu\text{m}$). Hence, the structure-functional change of LCA trees in mice of >8 months is mainly attributed to the regression of blood vessels (blood volumes of 7.1 ± 4.1 , 9.9 ± 3.7 , 16.1 ± 4.7 , and 13.8 ± 4.0 vs. 5.5 ± 3.4 ($\times 10^{-4}$) cm^3).

On the other hand, we showed the linear relationship between bifurcation angles and D_s/D_l in LCA trees of mice at ages of 3 and 6 weeks, but the parabolic curve with the peak bifurcation angles ($\sim 90^\circ$) at $D_s/D_l = 0.5$ in mice at ages of 12 weeks, 5-6

months and > 8 months. The linear relationship may be caused by the progression of mouse heart during juvenile growth while the parabolic curve is associated with the mature and stable heart size during adult growth, which requires further investigations with considering how the spatial heterogeneity of myocardial flows is altered by the age-dependent bifurcation angles.

Critique of the Study

The present study carried out the pulsatile blood flow analysis in coronary arterial trees of mice during normal juvenile and adult growth, which brings in some complexities. For example, although coronary arterial trees with diameter > 40 μm were reconstructed from μCT images, symmetric arteriolar subtrees with diameters from 40 μm down to the first capillaries were generated from two scaling relationships. The simple Womersley-type model was derived for Newtonian fluids in straight pipes. Here, the non-Newtonian effect was partly captured in small arteries by using a diameter-dependent viscosity. Based on a more realistic model with considering non-Newtonian fluids, the hemodynamic analysis should be performed to accurately validate morphometric predictions when arteriolar trees with diameter <40 μm are available. Moreover, the following studies should relate vessel tone and metabolic signals to the 3D spatial bifurcation asymmetry for understanding the microcirculation and myocardial heterogeneity deeply.

CONCLUSIONS

This study analyzed the morphometric and hemodynamic variation of microvascular bifurcations in LCA trees of normal mice at ages of 3, 6, 12 weeks, 5-6 months and >8 months. The inlet flow rate and blood volume of LCA trees increase during juvenile growth and decrease during adult growth while the flow waveform is preserved in diastole in the absence of vessel tone. The blood flow becomes more uniform as vessel diameters decrease from the inlet to 40 μm owing to the changes of diameter ratios (D_l/D_m and D_s/D_m). The changes of diameter ratios and AER also lead to an abrupt decrease of velocity ratios with the decrease of vessel diameter from 140 to 40 μm . Mice of >8 months show structure-functional difference from others.

AUTHOR CONTRIBUTIONS

The data analysis was done by YF, XW, TF, and XS. Micro-CT images were collected by LL, WZ, and MC. The manuscript was drafted and revised by YH, JLi and JLi.

ACKNOWLEDGMENTS

We would like to thank all participants in Peking University. The study is supported in part by the National Natural Science Foundation of China Grant 11672006, China MOST Grant 2014DFG32740 (YH), and Shenzhen Science and Technology R&D Grant JCYJ20160427170536358 (YH), and Capital's Funds for Health Improvement and Research 2016-2-4073 (JLi).

REFERENCES

- Arpino, J. M., Nong, Z. X., Li, F. Y., Yin, H., Ghonaim, N., Milkovich, S., et al. (2017). Four-Dimensional microvascular analysis reveals that regenerative angiogenesis in ischemic muscle produces a flawed microcirculation. *Circ. Res.* 120, 1453–1465. doi: 10.1161/CIRCRESAHA.116.310535
- Asakura, T., and Karino, T. (1990). Flow patterns and spatial distribution of atherosclerotic lesions in human coronary arteries. *Circ. Res.* 66, 1045–1066
- Baish, J. W., and Jain, R. K. (2000). Fractals and cancer. *Cancer Res.* 60, 3683–3688.
- Bejan, A., and Lorente, S. (2010). The constructal law of design and evolution in nature. *Philos. Trans. R. Soc. Lond. B Biol. Sci.* 365, 1335–1347. doi: 10.1098/rstb.2009.0302
- Carmeliet, P., and Jain, R. K. (2011). Molecular mechanisms and clinical applications of angiogenesis. *Nature* 473, 298–307. doi: 10.1038/nature10144
- Chen, X., Gao, Y., Lu, B., Jia, X., Zhong, L., Kassab, G. S., et al. (2016). Hemodynamics in coronary arterial tree of serial stenoses. *PLoS ONE* 11:e0163715. doi: 10.1371/journal.pone.0163715
- Chen, X., Niu, P., Niu, X., Shen, W., Duan, F., Ding, L., et al. (2015). Growth, ageing and scaling laws of coronary arterial trees. *J. R. Soc. Interface* 12:20150830. doi: 10.1098/rsif.2015.0830
- Chilian, W. M. (1991). Microvascular pressures and resistances in the left ventricular subepicardium and subendocardium. *Circ. Res.* 69, 561–570
- Chilian, W. M., Layne, S. M., Klausner, E. C., Eastham, C. L., and Marcus, M. L. (1989). Redistribution of coronary microvascular resistance produced by dipyridamole. *Am. J. Physiol.* 256(2 Pt 2), H383–H390. doi: 10.1152/ajpheart.1989.256.2.H383
- Chiu, J. J., and Chien, S. (2011). Effects of disturbed flow on vascular endothelium: pathophysiological basis and clinical perspectives. *Physiol. Rev.* 91, 327–387. doi: 10.1152/physrev.00047.2009
- Fan, T., Lu, Y., Gao, Y., Meng, J., Tan, W., Huo, Y., et al. (2016). Hemodynamics of left internal mammary artery bypass graft: effect of anastomotic geometry, coronary artery stenosis, and postoperative time. *J. Biomech.* 49, 645–652. doi: 10.1016/j.jbiomech.2016.01.031
- Gompper, G., and Fedosov, D. A. (2016). Modeling microcirculatory blood flow: current state and future perspectives. *Wiley Interdiscip. Rev. Syst. Biol. Med.* 8, 157–168. doi: 10.1002/wsbm.1326
- Huo, Y., Cheng, Y., Zhao, X., Lu, X., and Kassab, G. S. (2012b). Biaxial vasoactivity of porcine coronary artery. *Am. J. Physiol. Heart Circ. Physiol.* 302, H2058–H2063. doi: 10.1152/ajpheart.00758.2011
- Huo, Y., Choy, J. S., Svendsen, M., Sinha, A. K., and Kassab, G. S. (2009b). Effects of vessel compliance on flow pattern in porcine epicardial right coronary arterial tree. *J. Biomech.* 42, 594–602. doi: 10.1016/j.jbiomech.2008.12.011
- Huo, Y., Finet, G., Lefevre, T., Louvard, Y., Moussa, I., and Kassab, G. S. (2012a). Which diameter and angle rule provides optimal flow patterns in a coronary bifurcation? *J. Biomech.* 45, 1273–1279. doi: 10.1016/j.jbiomech.2012.01.033
- Huo, Y., Guo, X., and Kassab, G. S. (2008). The flow field along the entire length of mouse aorta and primary branches. *Ann. Biomed. Eng.* 36, 685–699. doi: 10.1007/s10439-008-9473-4
- Huo, Y., Kaimovitz, B., Lanir, Y., Wischgoll, T., Hoffman, J. I., and Kassab, G. S. (2009a). Biophysical model of the spatial heterogeneity of myocardial flow. *Biophys. J.* 96, 4035–4043. doi: 10.1016/j.bpj.2009.02.047
- Huo, Y., and Kassab, G. S. (2006). Pulsatile blood flow in the entire coronary arterial tree: theory and experiment. *Am. J. Physiol. Heart Circ. Physiol.* 291, H1074–H1087. doi: 10.1152/ajpheart.00200.2006
- Huo, Y., and Kassab, G. S. (2012a). Intraspecific scaling laws of vascular trees. *J. R. Soc. Interface* 9, 190–200. doi: 10.1098/rsif.2011.0270
- Huo, Y., and Kassab, G. S. (2012b). Compensatory remodeling of coronary microvasculature maintains shear stress in porcine left-ventricular hypertrophy. *J. Hypertens.* 30, 608–616. doi: 10.1097/HJH.0b013e32834f44dd
- Huo, Y., and Kassab, G. S. (2016). Scaling laws of coronary circulation in health and disease. *J. Biomech.* 49, 2531–2539. doi: 10.1016/j.jbiomech.2016.01.044
- Huo, Y. L., Finet, G., Lefevre, T., Louvard, Y., Moussa, I., and Kassab, G. S. (2012). Optimal diameter of diseased bifurcation segment: a practical rule for percutaneous coronary intervention. *EuroIntervention* 7, 1310–1316. doi: 10.4244/EIJV7I11A206
- Huo, Y., Linares, C. O., and Kassab, G. S. (2007b). Capillary perfusion and wall shear stress are restored in the coronary circulation of hypertrophic right ventricle. *Circ. Res.* 100, 273–283. doi: 10.1161/01.RES.0000257777.83431.13
- Huo, Y., Wischgoll, T., and Kassab, G. S. (2007a). Flow patterns in three-dimensional porcine epicardial coronary arterial tree. *Am. J. Physiol. Heart Circ. Physiol.* 293, H2959–H2970. doi: 10.1152/ajpheart.00586.2007
- Jacob, M., Chappell, D., and Becker, B. F. (2016). Regulation of blood flow and volume exchange across the microcirculation. *Crit. Care* 20:319. doi: 10.1186/s13054-016-1485-0
- Kaimovitz, B., Huo, Y., Lanir, Y., and Kassab, G. S. (2008). Diameter asymmetry of porcine coronary arterial trees: structural and functional implications. *Am. J. Physiol. Heart Circ. Physiol.* 294, H714–H723. doi: 10.1152/ajpheart.00818.2007
- Kassab, G. S. (2005). Functional hierarchy of coronary circulation: direct evidence of a structure-function relation. *Am. J. Physiol. Heart Circ. Physiol.* 289, H2559–H2565. doi: 10.1152/ajpheart.00561.2005
- Kleinstreuer, C., Hyun, S., Buchanan, J. R., Longest, P. W., Archie, J. P., and Truskey, G. A. (2001). Hemodynamic parameters and early intimal thickening in branching blood vessels. *Crit. Rev. Biomed. Eng.* 29, 1–64. doi: 10.1615/CritRevBiomedEng.v29.i1.10
- LeBlanc, A. J., and Hoying, J. B. (2016). Adaptation of the coronary microcirculation in aging. *Microcirculation* 23, 157–167. doi: 10.1111/micc.12264
- Malek, A. M., Alper, S. L., and Izumo, S. (1999). Hemodynamic shear stress and its role in atherosclerosis. *JAMA* 282, 2035–2042.
- Pries, A. R., Neuhaus, D., and Gaetgens, P. (1992). Blood viscosity in tube flow: dependence on diameter and hematocrit. *Am. J. Physiol.* 263(6 Pt 2), H1770–H1778. doi: 10.1152/ajpheart.1992.263.6.H1770
- Pries, A. R., and Secomb, T. W. (2005). Microvascular blood viscosity *in vivo* and the endothelial surface layer. *Am. J. Physiol. Heart Circ. Physiol.* 289, H2657–H2664. doi: 10.1152/ajpheart.00297.2005
- Pries, A. R., Secomb, T. W., and Gaetgens, P. (1995). Design Principles Of Vascular Beds. *Circ. Res.* 77, 1017–1023
- Reglin, B., Secomb, T. W., and Pries, A. R. (2017). Structural control of microvessel diameters: origins of metabolic signals. *Front. Physiol.* 8:813. doi: 10.3389/fphys.2017.00813
- Secomb, T. W. (2017). Blood flow in the microcirculation. *Annu. Rev. Fluid Mech.* 49, 443–461. doi: 10.1146/annurev-fluid-010816-060302
- Teng, B., Tilley, S. L., Ledent, C., and Mustafa, S. J. (2016). *In vivo* assessment of coronary flow and cardiac function after bolus adenosine injection in adenosine receptor knockout mice. *Physiol. Rep.* 4:e12818. doi: 10.14814/phy2.12818
- VanBavel, E., and Spaan, J. A. (1992). Branching patterns in the porcine coronary arterial tree. Estimation of flow heterogeneity. *Circ. Res.* 71, 1200–1212
- Wei, J. Y. (1992). Age and the cardiovascular system. *N. Engl. J. Med.* 327, 1735–1739
- Yin, X., Huang, X., Feng, Y., Tan, W., Liu, H., and Huo, Y. (2016). Interplay of proximal flow confluence and distal flow divergence in patient-specific vertebrobasilar system. *PLoS ONE* 11:e0159836. doi: 10.1371/journal.pone.0159836

Conflict of Interest Statement: The authors declare that the research was conducted in the absence of any commercial or financial relationships that could be construed as a potential conflict of interest.

Copyright © 2018 Feng, Wang, Fan, Li, Sun, Zhang, Cao, Liu, Li and Huo. This is an open-access article distributed under the terms of the Creative Commons Attribution License (CC BY). The use, distribution or reproduction in other forums is permitted, provided the original author(s) and the copyright owner are credited and that the original publication in this journal is cited, in accordance with accepted academic practice. No use, distribution or reproduction is permitted which does not comply with these terms.